TOWARDS THE DEVELOPMENT OF A NEW MODEL FOR THE OCULOMOTOR SYSTEM

G. Gibertoni, S. Cattini, and L. Rovati

University of Modena and Reggio Emilia, Department of Engineering "Enzo Ferrari"
Via P. Vivarelli 10, 41125 Modena, Italy

ABSTRACT

Pupillary light reflex involves many sensory and motor functions of the eye. For this reason, it represents an important emergency diagnostic tool and provides information to assess brain stem function. The pupil system can be considered in terms of input-output black-box behavior: light stimuli can be easily applied to the eyes, and the pupil size can be measured effortlessly and non-invasively.
In this paper, a model for short-light-flash-induced transient pupillary light reflex is presented and preliminary experiments designed to test the model features are described. Results confirm that the developed pupillary light reflex model is suitable to describe the pupil oculomotor system exposed to short-light flashes.

Keywords: Pupil Light Reflex, Pupil Model, Pupil Light Response, Ocular Imaging, Ophthalmic Diagnostic Tools, Ophthalmic Measurements, Biomedical Instrumentation, Optical Instrumentation.

1. INTRODUCTION

Pupillary light reflex (PLR) is the process that governs the changes in the pupil area in response to the illuminance variations. This process guarantees a correct illumination of the retina and a human vision that extends over several orders of magnitude in environmental illumination. PLR involves many important intracranial and neural pathways, as constriction and dilation phases of the pupil are a function of both parasympathetic and sympathetic divisions of the autonomic nervous system.[1]
Several studies have been conducted over the past decades on the PLR and many mathematical models have been proposed and validated with experimental data. Starting in the '20s, Reeves[2] and lately Moon and Spencer[3] successfully modeled steady-state pupil size as a function of log-light intensity. Lately, some dynamic models of PLR have been proposed by Sun,[4] Stark,[5] and more recently from Pamplona[6] and Privitera.[7] Fun et al. have successfully modeled, with superior results, PLR under specific light stimulation.[8]
Using a control theory-based approach, the pupil oculomotor-nervous system can be considered as a simple black-box with one input and one output: light stimuli, i.e. input, with a wide range of characteristics, can be easily applied to the eyes while the pupil size, i.e. output, variations can be measured effortlessly and non-invasively. The easy acquisition of PLR data allows many types of quantitative experiments to be conducted without causing unwanted stress on human subjects. The combination of all these elements makes the PLR analysis of great interest in many clinical procedures.[7]
In this paper, a physiological model suitable to describe the pupil oculomotor system exposed to short-light-flashes is presented. The model consists of one second-order differential equation and, potentially, allows extracting the autonomic nervous inputs and the dynamic characteristics of the pupil oculomotor system from PLR Data.

2. MODEL FOR THE HUMAN PUPILLARY MUSCLE PLANT

According to the control theory, PLR can be modeled as a single-input single-output dynamic system. As discussed in the literature,[7] this simple bio-mechanical system is characterized by many non-linearities as it involves different types of photoreceptors, as well as different neuroanatomical pathways, and thus its description in terms of closed-form equations is difficult.
Since the iris-muscle plant is essential throughout the control process, our model analyzes in detail this plant with reference to a bio-mechanical equivalence. In this context, PLR can be observed in response to well-defined transient light stimulation. In fact, under this type of stimulation,[8,9] it is possible to model the pupil response

by considering, as the main contribution, the mechanical properties of the iris-muscle plant.
From the mechanical point of view, the iris movement is governed by three forces: passive elastic forces, viscous resistance forces, and active forces generated by the parasympathetic and sympathetic modulation. In particular, the sphincter and dilator muscles control the pupil size. As schematically shown in Figure 1, the action of these two muscles can be modeled as two antagonist viscous-elastic elements. The viscous-elastic model described in

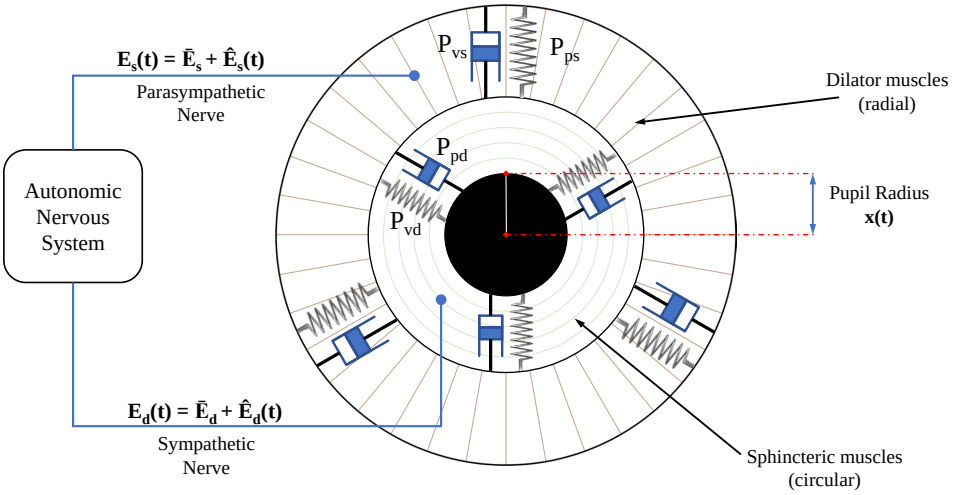

Figure 1: Schematic diagram of the human pupillary muscle plant. $E_s(t)$ and $E_d(t)$ are the parasympathetic and sympathetic nervous activities, respectively. $\bar{E}$ and $\hat{E}$ are the DC and AC components of the inputs, respectively. The radial, i.e. dilator, and circular, i.e. sphincter, muscles are mechanically described by a spring and dump couple, where P_{vs} and P_{vd} are the viscous components, while P_{ps} and P_{pd} are the elastic ones.

detail by Hirata et al.[9,10] was used as starting point for this work. In this model, the parasympathetic $E_s(t)$ and sympathetic $E_d(t)$ nervous activities, which directly innervate the sphincter and dilator muscles, are considered as the inputs of the control system. The muscles activities are then expressed with three main functions: passive elastic forces (subscript $_p$), viscous resistance forces (subscript $_v$), and active tensor forces(subscript $_a$) according to the following equations;[9] here parameters with subscript $_s$ state for sphincter muscles, while parameters with subscript $_d$ refer to dilator. Moreover, static and dynamic components are marked with overline $\bar{}$ and a circumflex $\hat{}$ symbols, respectively.

Passive Elastic Forces:

$$P_p = \begin{cases} a(z-l_0)^4 + b(z-l_0)^2, & (z \geq l_0) \\ 0, & (z < l_0) \end{cases} \tag{1}$$

where z is the muscle length, a and b are two constants, and l_0 is the muscle length at rest.

Viscous Resistance Forces:

$$P_v = \begin{cases} D_+ \frac{dz}{dt}, & (\frac{dz}{dt} \geq 0) \\ D_- \frac{dz}{dt}, & (\frac{dz}{dt} < 0) \end{cases} \tag{2}$$

where $\frac{dz}{dt}$ is the muscle length variation velocity. D_+ and D_- are two viscous coefficients of resistance during the stretch and release phases of the muscle, respectively.

Active Tensor Forces:

$$P_a = \left(\bar{E} + \hat{g}(t)\right) \cdot p_a(z) \tag{3}$$

$$p_a(z) = \begin{cases} P_0 - c(z - L_0)^2, & (P_0 \geq c(z - L_0)^2) \\ 0, & (P_0 < c(z - L_0)^2) \end{cases} \tag{4}$$

$$\frac{d^2\hat{g}(t)}{dt^2} + (2\alpha + \beta)\frac{d\hat{g}(t)}{dt} + \alpha(\alpha + \beta)\hat{g}(t) = \beta\hat{E}(t - t_D) \tag{5}$$

where c is a constant, L_0 is the length of the muscle at which the maximum tension P_0 is generated. $p_a(z)$ and $\hat{g}(t)$ are muscle length-dependent and input dependent components of the dynamic active tension, respectively. α and β are the negative and positive time constants of the tensor isometric response, respectively. $\hat{E}$ and $\bar{E}$ are the AC and DC input components coming from the autonomic nervous system. The delay time of the nervous response $\hat{E}$ is described by the time interval t_D. The two model inputs, i.e. parasympathetic and sympathetic nervous activities, are expressed as follow:

$$\begin{aligned} E_s(t) &= \bar{E}_s + \hat{E}_s, \;\; E_s(t) \geq 0 \\ E_d(t) &= \bar{E}_d + \hat{E}_d, \;\; E_d(t) \geq 0 \end{aligned} \tag{6}$$

The reciprocal relation for both nervous activities at equilibrium must be also considered; thus the static input nervous activities must be balanced as follow:

$$\bar{E}_d = 1 - \bar{E}_s, 0 \leq \;\; \bar{E}_s \leq 1 \tag{7}$$

In conclusion, opposite tensions and forces of the one-dimensional structure muscle configuration have been combined:

$$m \cdot \frac{d^2x}{dt^2} = P_{pd} + P_{ad} - P_{ps} - P_{as} - P_{vd} - P_{vs} \tag{8}$$

where m is the total mass of the moving muscles and x is the pupil radius. As $x(t)$ is considered as the model output, sphincter and dilator muscle length of Equations 1 and 4 have been adjusted accordingly. According to Usui et al.,[9] sphincter and dilator muscle length can be described for this model as:

$$\begin{aligned} z_d &= x_{max} - x \\ z_s &= x \end{aligned} \tag{9}$$

where z_d and z_s are dilator and sphincter muscle length, respectively, whereas x_{max} is the pupil radius at brain death. The model and all the derived functions, together with all the parameters that describe the two muscles behavior were implemented in the Matlab-Simulink© environment. In Section 4, the autonomic nervous inputs and all the muscles parameters have been extracted from PLR Data.

3. MATERIALS AND METHODS

To understand autonomic nervous activities and dynamic mechanical properties characterizing the PLR, preliminary experiments were performed on human volunteers.

The experiments were performed using a custom binocular pupillometer that was developed modifying a VR (Virtual Reality) Headset.[11] This pupillometer uses the VR lenses to ensure a correct Maxwellian-like eye illumination.[12] In such a way, variations of pupil size do not alter the total amount of light impinging the retina.[13] Pupil size was measured at 24 fps using two infrared cameras fixed on the VR display plane.

The experiment was performed observing the PLR response to green short light flashes on two male human volunteers A and B aged 26 and 55 years, respectively. Using transit stimulation, the autonomic nervous innervation activities, described in Eq. 6, can be assumed to have the same temporal waveform of luminous flux intensities with additional time delays.[9] Figure 2 shows a schematic diagram of the assumed autonomic nervous activities in response to a short light pulse.

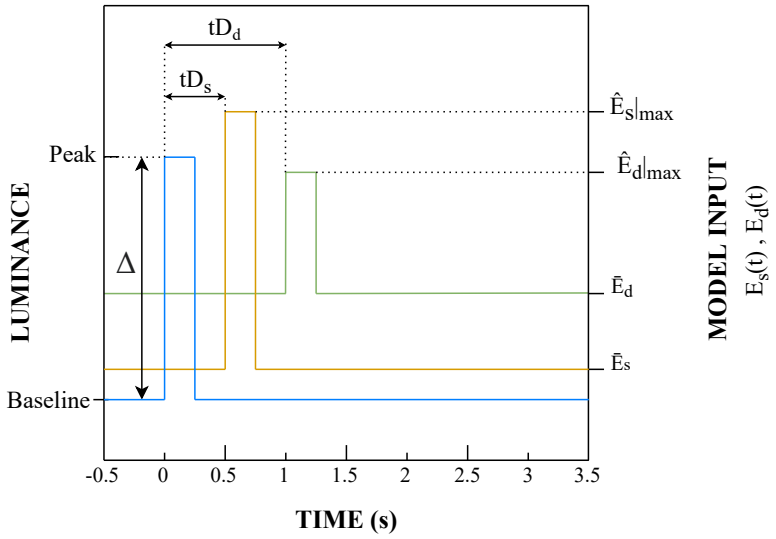

Figure 2: Schematic diagram of autonomic nervous activities in response to a short light flash. $E_s(t)$ and $E_d(t)$ are the parasympathetic and sympathetic nervous activities, respectively.

As shown in Figure 3, each experiment consisted of three different light stimulation phases. The first phase lasted 2 minutes with all light sources turned OFF. Luminous flux in this phase was comparable to a dark room during the daylight. This initial dark adaptation is essential to decouple the photoreceptor's excitation conditions from the external environment. In the second phase, a steady luminous flux equal to the *baseline* value was presented for 2 minutes. This phase assured that the photoreceptors reached properly the *baseline* excitation level. In the last phase, a total of 30 flashes of 250 ms width and five seconds interval period were presented to the stimulated eye.

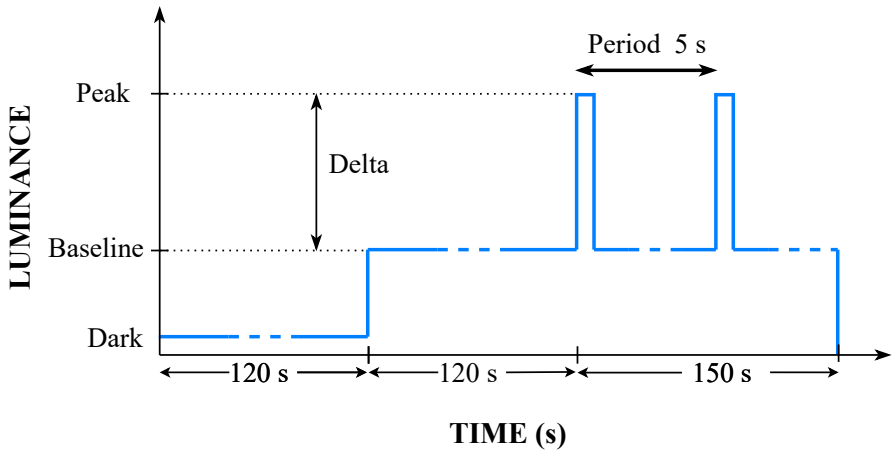

Figure 3: Experimental temporal phases: (i) two minutes of dark adaptation, (ii) two minutes of baseline adaptation, and (iii) 30 green flashes of 250 ms duration and with 5 seconds interval period.

The light stimulus was generated by a set of green LEDs, with peak emission at 528 nm, FWHM of 27 nm; thanks to the LEDs spatial distribution and the VR optics, the stimulus illuminated uniformly the retina in a field of view (FOV) of about 45 degrees.
Three different tests were performed for each of the two volunteers stimulating the right eye. To minimize the effect of other physiological reactions that could alter the normal state of activity of the pupil, each test consisted of two sets of measurements acquired on two different days. Moreover, the measurements were carried out in a dark and noise-free environment, between 11:00 and 12:00 am. Luminous flux levels of the baseline and peak for the three experiments are shown in Table 1.

	Baseline (mlm)	**Peak (mlm)**	**Delta Δ (mlm)**
Experiment 1	0.753	6.100	5.347
Experiment 2	3.900	5.900	2.000
Experiment 3	3.900	9.600	5.700

Table 1: Luminous flux levels of the baseline and peak for the three experiments.

Note as the experiments 1 and 2, the light stimulus had approximately the same peak luminous flux but different baseline values. Experiments 2 and 3 shared the same baseline luminous flux while the last one had a higher peak luminous flux. In experiments 1 and 3, the light stimulus had almost the same amplitude, i.e. Δ. These stimuli were selected to highlight possible correlations among model parameters estimated for different autonomic nervous system excitation levels.

4. PRELIMINARY RESULTS AND DISCUSSION

Figure 4 shows the average experimental response recorded during the experiments. The inverse aforementioned model was used to fit the experimental data. The obtained by fitting curves are shown in the same figure. The PLR responses, i.e. dashed blue lines, were obtained with a boxcar average over the 30 flash responses. Temporal alignment of the responses was possible thanks to system-integrated photodiodes that generated a reference signal. As showed in Figure 2, light flash rising edge take place at time instant $t = 0$ s also in graphs of Figure 4. The model fitting was then computed for the PLR responses applying some mechanical and physiological constraints. Mechanical constraints are strictly related to nature and physical functioning of the pupillary response, and are reported last column of Table 2. The fitting was performed by a nonlinear least square method with *trust-region-reflective* algorithm integrated in the parameter estimation toolbox provided with Simulink© R2020b. Fittings were set to minimize the sum square error of each PLR response. The estimated parameters of our

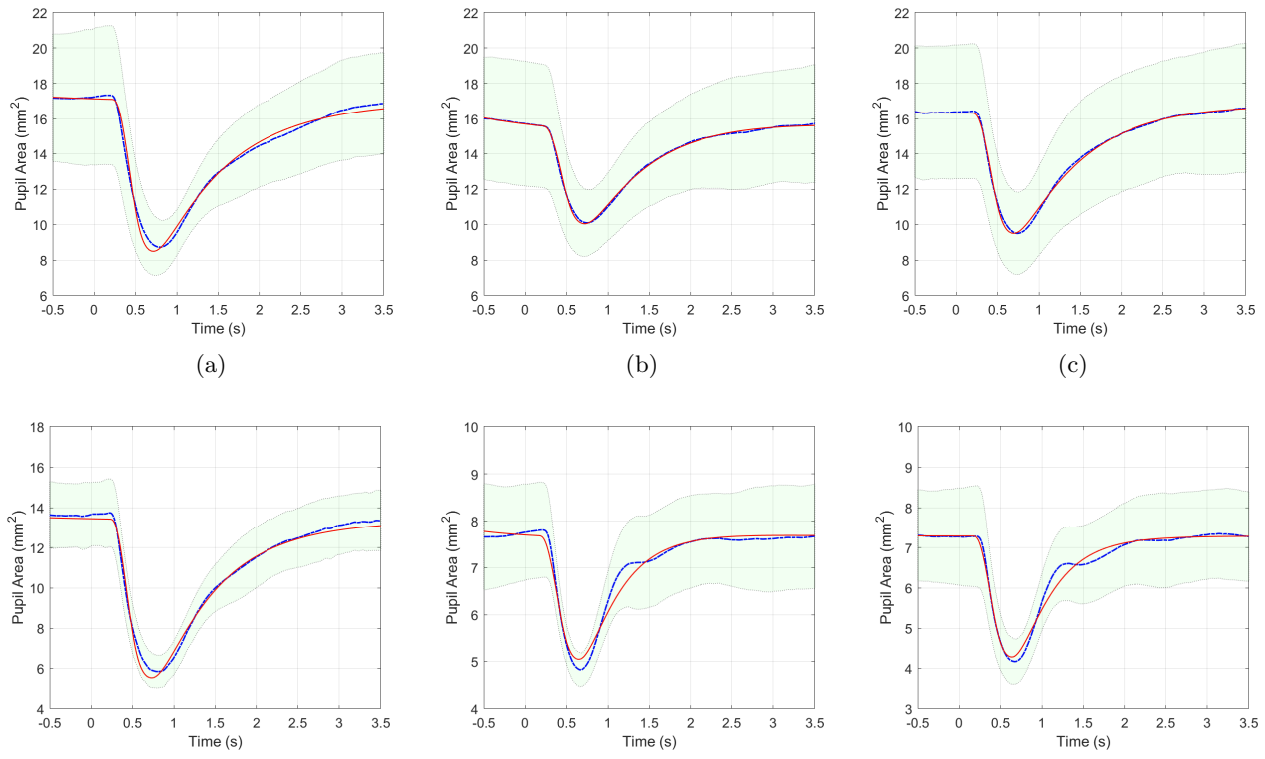

Figure 4: (a), (b) and (c) shows the pupil response of subject A to experiments 1, 2 and 3, respectively. (d), (e) and (f) show the pupil response of subject B to experiments 1, 2 and 3, respectively. Blue dashed lines are the average experimental pupil response. Light green regions represent the standard deviation of the mean. Solid red lines show the best fit results obtained from our model.

model for the two subjects considering the three experiments performed are summarized in Table 2. Parameters not dependent on the input light stimuli, strictly related to physiological/mechanical properties of the subject eye, were estimated once for each subject. Due to the correlation to the activity of the autonomic nervous system, the input-dependant variables instead, highlighted in Table 2, were computed for each experiment. Looking at the estimated parameters, it is worth noting that both subjects have similar mechanical/physical properties of the muscle plant, with minor differences in muscle lengths at rest ($l0_d$ and $l0_s$) and pupil sizes at brain death (A_{max}). Subject A presented a slightly faster sphincter contraction time (α_s) but a significantly slower sphincter release time (β_s). This is also well visible in the pupil response in Figure 4: a slightly steeper contraction slope but evidently a smoother and slower pupil dilation phase in respect to subject B, especially in experiments 2 and 3.

Considering the input dependant estimated parameters, the dynamic parasympathetic nervous activity, i.e. $\hat{E}_s|_{max}$, is the highest in both subjects in experiment 1 and the lowest in experiment 2, even if the peak luminous flux was roughly the same. This is probably due to a larger stimulus amplitude, i.e. Δ. Although experiment 3 exploited a stimulus amplitude similar to experiment 1, the parasympathetic nervous activity is less consistent. This is also well visible in Figures 4c and 4f, variations in the pupillary area are lower in experiment 3 for both subjects. This is probably related to the initial excitation status of the oculomotor system that approaches the saturation level for the higher baseline luminous flux used in experiment 3.

Concerning the parasympathetic static activity, i.e. Es_{stat}, the fitting results show a consistently higher value in experiments 2 and 3 for subject B. Besides, the dynamic component of sympathetic activity, ($\hat{E}_d|_{max}$), is negligible for the first experiment but is significant in the other two experiments for both subjects. This is, again, probably related to the higher baseline excitation that, in turn, determines the initial pupil condition,

Model Parameters	SUBJECT A			SUBJECT B			Fitting Constrains
	Exp1	Exp2	Exp3	Exp1	Exp2	Exp3	
a_d	5.700			5.968			$a_d \geq 0$
a_s	4.320			4.318			$a_s \geq 0$
b_d	31.228			32.023			$b_d \geq 0$
b_s	11.775			11.686			$b_s \geq 0$
c_d	9.319			6.295			$c_d \geq 0$
c_s	128.030			127.270			$c_s \geq 0$
$\alpha_d(1/s)$	0.275			0.275			$\alpha_d \geq 0$
$\alpha_s(1/s)$	8.966			8.038			$\alpha_s \geq 0$
$\beta_d(1/s)$	5.576			5.576			$\beta_d \geq 0$
$\beta_s(1/s)$	5.024			8.331			$\beta_s \geq 0$
$D_-(mN/mm/s)$	173.450			199.970			$D_- \geq 0$
$D_+(mN/mm/s)$	120.450			103.350			$D_+ \geq 0$
$L0_d(mm)$	2.897			2.856			$L0_d > l0_d$
$l0_d(mm)$	1.392			1.832			$l0_d \geq 0$
$L0_s(mm)$	3.751			3.699			$L0_s > l0_s$
$l0_s(mm)$	2.000			1.760			$l0_s \geq 0$
$P0_d(mN)$	396.600			373.130			≥ 0
$P0_s(mN)$	1177.500			1209.700			≥ 0
$A_{max}(mm^2)$	47.051			44.914			$A_{max} \leq \pi X_{max}^2$
$A_{ini}(mm^2)$	17.217	16.046	16.331	13.515	7.778	7.296	$A_{max} \geq A_{ini} \geq \pi X_{min}^2$
$\bar{E}s(a.u.)$	0.260	0.265	0.261	0.295	0.377	0.385	$1 \geq \bar{E}s \geq 0$
$\hat{E}_d\|_{max}(a.u.)$	≈ 0	0.166	0.125	≈ 0	0.046	0.052	$\hat{E}_d \geq 0$
$\hat{E}_s\|_{max}(a.u.)$	20.136	12.161	16.573	19.810	10.661	14.588	$\hat{E}_s \geq 0$
$tD_d(s)$	0.572	0.546	0.405	0.698	0.401	0.503	$tD_d \geq tD_s$
$tD_s(s)$	0.218	0.207	0.200	0.228	0.175	0.172	$tD_s \geq 0$

Table 2: Fitted parameters from the model outputs in Figure 4. A_{max} is the estimated pupil area at brain death whereas A_{ini} represents the pupil area at the initial condition in each experiment. X_{max} and X_{min} are pupil radius maximum and minimum allowable values.

i.e. A_{ini}. Regarding the nervous activity delay times, it is worth noting that the sphincter reaction time, tD_s is slightly lower if the baseline excitation level is higher, especially for subject B.
Table 3 reports the sum squared errors of the fitting; these low error values prove as the analyzed physical model adequately fits the experimental data for the considered short-light-flash stimuli. The average coefficient of determination among all six experiments, i.e. R^2, is about 0,86. Low-frequency fluctuations in pupil size, commonly present in the oculomotor system of the human eye, can affect the boxcar averaging results reducing the fitting accuracy. Another variable that can affect the fitting results could be the assumptions used to model the input signal from the autonomic nervous system explained previously in Figure 2.

	Sum Squared Errors (SSE)	
	SUBJECT A	SUBJECT B
Eperiment 1	0.1603	0.1490
Eperiment 2	0.0162	0.2476
Eperiment 3	0.0322	0.2381

Table 3: Sum squared errors of the model fitting for the three experiments.

5. CONCLUSIONS

A preliminary study towards the development of a new model for the iris oculomotor system has been described. The developed model for short-light-flash-induced transient PLR showed the right features to describe the iris oculomotor system exposed to such types of stimuli. Many other experiments need to be conducted to fully validate the model. In the near future, the definition of new methods and models for PLR analysis can pave the basis for more advanced diagnostic techniques that can be exploited to estimate optic-nervous system diseases.

REFERENCES

[1] Usui, S. and Stark, L., "A model for nonlinear stochastic behavior of the pupil," *Biol. Cybern.* **45**, 13–21 (Aug. 1982).

[2] Reeves, P., "The Response of the Average Pupil to Various Intensities of Light," *J. Opt. Soc. Am., JOSA* **4**, 35–43 (Mar. 1920). Publisher: Optical Society of America.

[3] Moon, P. and Spencer, D. E., "On the Stiles-Crawford Effect," *J. Opt. Soc. Am., JOSA* **34**, 319–329 (June 1944). Publisher: Optical Society of America.

[4] Sun, F., Tauchi, P., and Stark, L., "Dynamic pupillary response controlled by the pupil size effect," *Experimental Neurology* **82**, 313–324 (Nov. 1983).

[5] Stark, L. W., "The Pupil as a Paradigm for Neurological Control Systems," *IEEE Transactions on Biomedical Engineering* **BME-31**, 919–924 (Dec. 1984).

[6] Pamplona, V. F., Oliveira, M. M., and Baranoski, G. V. G., "Photorealistic models for pupil light reflex and iridal pattern deformation," *ACM Trans. Graph.* **28**, 106:1–106:12 (Sept. 2009).

[7] Privitera, C. M. and Stark, L. W., "A Binocular Pupil Model for Simulation of Relative Afferent Pupil Defects and the Swinging Flashlight Test," *Biological Cybernetics* **94**, 215–224 (Mar. 2006).

[8] Fan, X. and Yao, G., "Modeling Transient Pupillary Light Reflex Induced by a Short Light Flash," *IEEE Transactions on Biomedical Engineering* **58**, 36–42 (Jan. 2011).

[9] Usui, S. and Hirata, Y., "Estimation of autonomic nervous activity using the inverse dynamic model of the pupil muscle plant," *Annals of biomedical engineering* **23**(4), 375–387 (1995).

[10] Hirata, Y. and Usui, S., "A nonlinear dynamical model for human pupillary muscle plant," *Trans IEICE* **77**, 170–180 (1994).

[11] Gibertoni, G., *Design and realization of a binocular pupillometer for RGB flicker annoyance estimation*, master thesis dissertation, Università di Modena e Reggio Emilia (Apr. 2019).

[12] Sugawara, M., Suzuki, M., and Miyauchi, N., "14-5l: Late-news paper: Retinal imaging laser eyewear with focus-free and augmented reality," in [*SID Symposium Digest of Technical Papers*], **47**(1), 164–167, Wiley Online Library (2016).

[13] Westheimer, G., "The maxwellian view," *Vision research* **6**(11-12), 669–682 (1966).